Research Article
doi.org/10.1002/cctc.202201163

Chemistry Europe
European Chemical Societies Publishing

www.chemcatchem.org

Photocatalytic Reduction of CO_2 by Highly Efficient Homogeneous Fe^{II} Catalyst based on 2,6-Bis(1′,2′,3′-triazolyl-methyl)pyridine. Comparison with Analogues.

Lisa-Lou Gracia,[a] Elham Barani,[b] Jonas Braun,[c] Anthony B. Carter,[c] Olaf Fuhr,[b, d] Annie K. Powell,[b, c] Karin Fink,[b] and Claudia Bizzarri*[a]

Fully earth-abundant and highly efficient systems for producing syngas CO/H_2 through photocatalytic reduction from CO_2 are essential to approach a sustainable way of closing the carbon cycle. Herein, the synthesis and characterization of a new iron complex, $Fe^{II}L(NCS)_2py$, coordinated to an N,N,N-pincer ligand 2,6-bis(4′-phenyl-1′,2′,3′-triazol-1′-yl-methyl)pyridine (L), two isothiocyanate groups (NCS) and one pyridine is reported. Its catalytic activity in the photo-driven reduction of carbon dioxide has been investigated and compared with its Co^{II} analogue ($CoL(NCS)_2py$) and their homoleptic complexes ML_2. In this work, the catalysts are used in combination with the heteroleptic complex [Cu^{I}(dmp)(DPEphos)], where dmp is 2,9-dimethyl-1,10-phenanthroline and DPEPhos is bis[(2-diphenylphosphino)phenyl] ether, to reach entirely earth-abundant systems. The new iron heteroleptic complex $Fe^{II}L(NCS)_2py$ showed considerable activity with a TON_{CO} of 576 obtained after 4 h (TOF = 144 h^{-1}) through visible light ($\lambda = 420$ nm) and a quantum yield of 7.1 %.

Introduction

Natural photosynthesis removes carbon dioxide from the atmosphere and transforms it into biomass using solar light, the most abundant renewable energy available on earth. Each year, 7.6 billion metric tons of CO_2 are consumed by forests.[1] However, because of human activity, the balance of the carbon cycle is disturbed, leading to climate change and global warming. The photocatalytic reduction of carbon dioxide enables the use of a waste product of combustion as a starting material for organic chemical products.[2] Used on a large scale, this could re-balance the disturbed carbon cycle.[3] Almost forty years of research have been devoted to finding new and efficient systems for achieving this aim. In photo-driven CO_2 reduction,[4] a photosensitizer (PS) is needed to harvest the solar light and a catalyst (CAT) to reduce carbon dioxide. Both can be homogeneous or heterogeneous. A sacrificial electron donor (e-D) is added to close the catalytic cycle and regenerate the ground state of the photosensitizer. In homogeneous systems, both PS and CAT are mostly transition metal-based and rarely organic-based.[5],[6][7] Despite the excellent photochemical and electrochemical properties of noble metals (e.g. Ru, Ir, Re), ecofriendly alternative systems using 3d metals (e.g. Mn, Fe, Co, Ni) are becoming competitive.[8] Usually, 3d metals manifest only two possible oxidation states, leading to the formation of two-electrons reduction products such as carbon monoxide, formaldehyde, or formic acid. Molecular hydrogen is, in most cases, a coproduct, and the selectivity varies abundantly. A mixture of CO and H_2 as products, also known as syngas, constitutes an opportunity to generate fuels in a more ecological way,[9] either used as such (for fuel gas turbines)[10] or through further reaction (to produce methanol for example).[11] Efficient earth-abundant systems exploit catalysts based especially on iron and cobalt porphyrins[12] and multi-pyridine-based ligands,[13] although rare metal complexes are still predominantly used as PS. First examples, where an entire noble-metal free system was used for photo-driven CO_2 reduction, were presented using iron catalysts combined with copper-based photosensitizers.[14] In particular, the known complex [Fe^{II}-$(dmp)_2(NCS)_2$] (where dmp is 2,9-dimethyl 1,10-phenanthroline) was efficiently used as a catalyst with several heteroleptic Cu^{I} complexes as photosensitizers, achieving a maximum turnover number (TON) of 273 for CO production after 12 hours.[14b] The same catalyst was later used in a photocatalytic system that employed a more sophisticated version of the previously used Cu^{I} complex, and the TON_{CO} was 440 after 24 hours of

[a] L.-L. Gracia, Dr. C. Bizzarri
Institute of Organic Chemistry
Karlsruhe Institute of Technology (KIT)
Fritz-Haber-Weg 6, 76131 Karlsruhe (Germany)
E-mail: bizzarri@kit.edu
Homepage: https://www.ioc.kit.edu/bizzarri/english/index.php
[b] E. Barani, Dr. O. Fuhr, Prof. A. K. Powell, Prof. Dr. K. Fink
Institute of Nanotechnology (INT)
Karlsruhe Institute of Technology (KIT)
Hermann-von-Helmholtz-Platz 1,
76344 Eggenstein-Leopoldshafen (Germany)
[c] J. Braun, A. B. Carter, Prof. A. K. Powell
Institute of Inorganic Chemistry
Karlsruhe Institute of Technology (KIT)
Engesserstraße 15, 76131 Karlsruhe (Germany)
[d] Dr. O. Fuhr
Karlsruhe Nano Micro Facility (KNMFi)
Karlsruhe Institute of Technology (KIT)
Hermann-von-Helmholtz-Platz 1,
76344 Eggenstein-Leopoldshafen (Germany)

Supporting information for this article is available on the WWW under https://doi.org/10.1002/cctc.202201163

irradiation with a CO selectivity of 70%.[15] Other noble-metal-free systems have recently been developed and summarized in different reviews.[8d,13a,16]

Among all the transition metals of the first row, iron is the cheapest and the most abundant in the earth's crust (56,300 ppm).[17] It is also the most exciting metal to build efficient catalysts with, as its cost-effectiveness makes it appealing for large-scale applications. Thus, we aim to design and produce Fe^{II} complexes that can be used as CAT in photo-driven CO_2 reduction. Herein, we focus on the synthesis of a new heteroleptic iron complex based on a tridentate ligand, 2,6-bis-(4'-phenyl-1',2',3'-triazol-1'-yl-methyl) pyridine, two isothiocyanates, and a pyridine (py) (**1**, Figure 1). Furthermore, we prepared the corresponding cobalt-based heteroleptic complex ($CoL(NCS)_2py$, **2**) and the two homoleptic complexes ML_2 (where M = Fe, Co, in **3** and **4** respectively) and compared their activities as catalysts in photocatalytic carbon dioxide reduction. Their performance was tested in a noble-metal-free system by employing them with a Cu^{I} complex, Cu(dmp)(DPEPhos), where DPEPhos = bis[(2-diphenylphosphino)phenyl] ether[18] as the photosensitizer and 1,3-dimethyl-2-phenylbenzimidazoline (BIH) as the sacrificial electron donor. In particular, the photocatalytic system containing the very efficient heteroleptic Fe-based CAT **1** produced CO with a $TON_{CO} = 576$ only after 4 hours of irradiation at 420 nm, with a selectivity up to 70% for CO over H_2. The calculated quantum yields are encouraging at 7.1%. These values are comparable to some of the best-reported approaches using fully earth-abundant systems with Fe-based catalysts.

Results and Discussion

Synthesis and X-ray characterization

The N,N,N-pincer ligand 2,6-bis(4'-phenyl-1',2',3'-triazol-1'-yl-methyl)pyridine was prepared according to a known procedure[19] *via* a copper-alkyne-azide cycloaddition (CuAAC) from an *in situ* prepared 2,6-bis(azidomethyl)pyridine and phenylacetylene. Figure 1 schematically shows the synthesis of the heteroleptic $ML(NCS)_2py$ complexes (M = Fe, Co). $M(ClO_4)$ was used as the precursor for the synthesis of ML_2[19] while $M(NCS)_2py_4$ was employed to form the heteroleptic $ML(NCS)_2py$ complexes.

For the heteroleptic complexes, the ligand L was reacted with $M(NCS)_2py_4$ in MeOH at 20 °C for 2 h with 65% and 85% yields for **1** and **2**, respectively. For **3** and **4**, the perchlorate precursors were reacted for 30 minutes at 20 °C, giving excellent yields of 95% and 89%, respectively. The synthesis of **1** was performed under an inert atmosphere in a glovebox. The synthesis of the homoleptic ML_2 complexes was done following the procedure of Zhu *et al.*,[19] who in 2011 described and characterized homoleptic Fe^{II}, Co^{II}, and Cu^{II} complexes, using the same tridentate ligand.

Analogous homoleptic Fe^{II}, Ni^{II}, Co^{II} and Cu^{II} complexes were synthesized in 1990 by Mahapatra *et al.* using non-planar 2-(pyrazol-1-ylmethyl)pyridine ligands.[20] Moreover, Re(I) heteroleptic complexes have been synthesized by Crowley *et al.* using one L and three CO ligands.[21]

Suitable crystals for X-ray single crystal diffraction were grown for all complexes by slow diffusion of diethyl ether in concentrated solutions of acetonitrile (MeCN) at room temperature. (Figure 2) As expected from the literature, the homoleptic

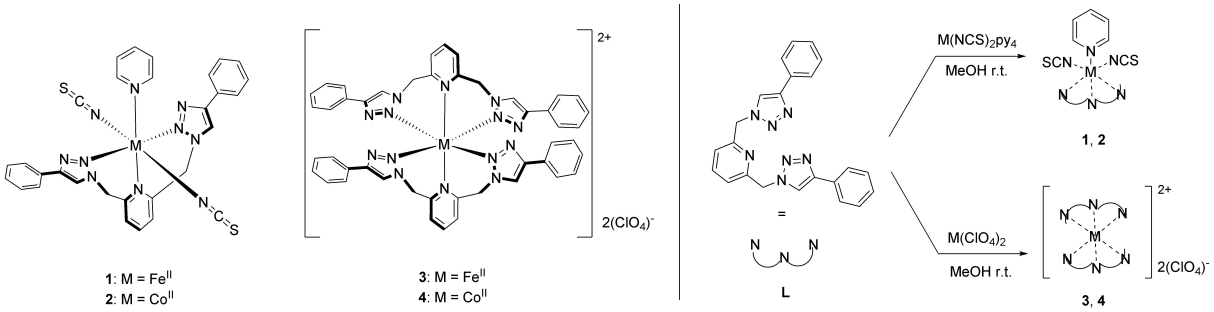

Figure 1. (Left) Chemical structures of the Fe^{II} and Co^{II} complexes investigated as CO_2 reduction CAT in this work. (Right) Synthetic pathways of the heteroleptic (**1** and **2**) and homoleptic (**3** and **4**) complexes in methanol at room temperature.

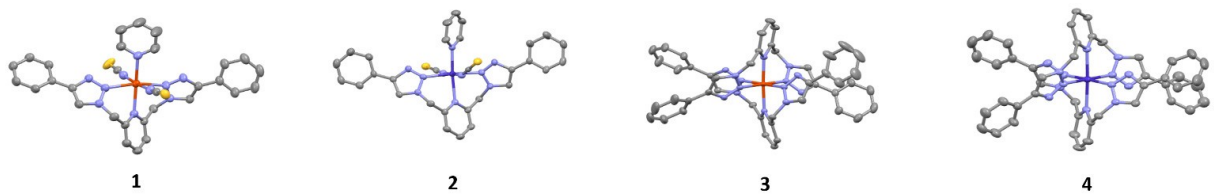

Figure 2. Molecular structures of the catalysts with 50% of probability thermal ellipsoids.

octahedral ML_2 perchlorate complexes **3** and **4** crystallize in the triclinic space group $P\bar{1}$.[19] Concerning the $ML(NCS)_2py$ complexes, both **1** and **2** crystallize in the monoclinic space group $P2_1/n$ with a distorted octahedral coordination geometry. The structures of **1** and **2** reveal that two thiocyanates and one pyridine ligand complete the coordination sphere of the metal center. Selected bond lengths and angles of **1** and **2** are summarized in Tables S4, S5, S6, and S7. M–L distances,[22] bond-valence sum analysis (Figures S12, S13, S14 and S15, Tables S4, S5, S6 and S7)[23] as well as the number of unpaired electrons, calculated by the Evans method (Figures S8, S9, S10 and S11, Tables S1, S2 and S3) allowed us to determine the oxidation and spin state of the metal centers. All metal ions are in the oxidation state +2 and it was found that **3** is in the diamagnetic low spin state (LS) in contrast to **4** being in the high spin state (HS) with three unpaired electrons. Concerning the new heteroleptic complexes, **1** has a high spin state with four unpaired electrons and **2** with three unpaired electrons. Moreover, compounds **2**, **3**, and **4** do not show any oxidation change upon air exposure. In contrast, **1** rapidly turns red on exposure to air, likely due to oxidation from Fe^{II} to Fe^{III}.

Electronic absorption and electrochemistry

The absorption spectra of the complexes in acetonitrile are shown in Figure 3. They all present similar characteristics except **2**, which reveals an additional band at 340 nm. This band corresponds to a transition involving the Co-NSC bond, also present in the absorption spectrum of the cobalt precursor. The complexes show high photostability in MeCN/TEOA upon white light exposure for 20 h (Figure S24).

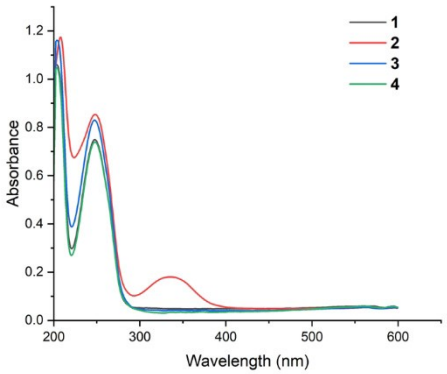

Figure 3. UV-vis absorption spectra of the catalysts (10^{-3} mM) in MeCN at 22 °C.

Table 1. Redox potentials of the catalysts and their reduction states reacting with CO_2.

Sample	E_{red}[a] [V]	CO_2 catalytic current onset[b]
1	−1.01; −1.76	−1.67
2	−1.23; −2.42	−1.78
3	−0.91; −1.63	−1.9
4	−1.81	−1.82

[a] Measured in MeCN/TEOA (5:1, v/v) at a scan rate of 100 mV s^{-1} and reported versus the ferrocene/ferrocenium couple. [b] Determined by DPV under CO_2 atmosphere.

Cyclic voltammetry and differential pulse voltammetry were performed in MeCN/TEOA (5:1, v/v) on all catalysts with 0.1 M tetrabutylammonium hexafluorophosphate ($TBAPF_6$) as supporting electrolyte. A glassy carbon disk was employed as the working electrode. The redox properties of the complexes are reported versus the internal standard Fc^+/Fc couple in Table 1, and the cyclic voltammograms are shown in Figure S16. The iron complexes **1** and **3** present similar features under Ar. The first reduction is quasi reversible and appears at −1.01 V and −0.91 V for **1** and **3**, respectively. This process is assigned to the Fe^{II} to Fe^{I} reduction. The second irreversible reduction occurs at lower potentials: −1.76 V (complex **1**) and −1.63 V (complex **3**).

This is assigned to the further reduction process from Fe^{I} to Fe^{0}. The heteroleptic Co^{II} complex **2** is reduced to Co^{I} at −1.23 V, and the process appears irreversible. The second reduction of the cobalt ion occurs at highly negative potentials so that it cannot be distinguished from the reduction process of the ligand, occurring at −2.42 V. The homoleptic cobalt complex **4** only shows one irreversible reduction at −1.81 V. Differential Pulse Voltammetry (DPV) of the four complexes gave similar results as the CV under argon atmosphere. However, when it was recorded under a CO_2 atmosphere, a different behavior could be observed, which is shown in Figure 4.

In fact, under a CO_2 atmosphere, iron complexes show a catalytic current after the second reduction at −1.67 V for **1** and −1.80 V for **3**. This suggests that the iron complexes must be in the typical reduced form of Fe^0 before they can coordinate and reduce CO_2, according to previous reports about iron catalysts for CO_2 reduction.[24] Similarly, the cobalt complexes **2** and **4** present a catalytic current after the first reduction, meaning that the reduced species Co^{I} reacts with CO_2. A further DPV experiment was performed by adding 0.1 mM of water to the solution containing **1**. In that case, the catalytic current observed in the DPV is slightly shifted from −1.67 V (without water) to a less negative potential of −1.59 V (Figure S21). In fact, water could act as a proton donor, facilitating the reaction. Nevertheless, the presence of water enhances the generation of the coproduct H_2, as shown in the photocatalytic experiments (*vide infra*).

Photocatalytic reduction of CO_2

The activity of our new catalyst $FeL(NCS)_2py$ and its analogue complexes in the photo-driven reduction of carbon dioxide was evaluated in combination with $[Cu^{I}(dmp)(DPEPhos)](BF_4)$ as photosensitizerand BIH as the electron donor. The photocatalytic experiments were carried out by dissolving all the components in a 4.0 mL mixed solution of MeCN and triethanolamine (TEOA) in a 5:1 ratio under irradiation at 420 nm for 4 hours. The concentration of CAT, PS, and BIH was fixed at 0.1 mM, 1.0 mM, and 20 mM, respectively. Analyses of the

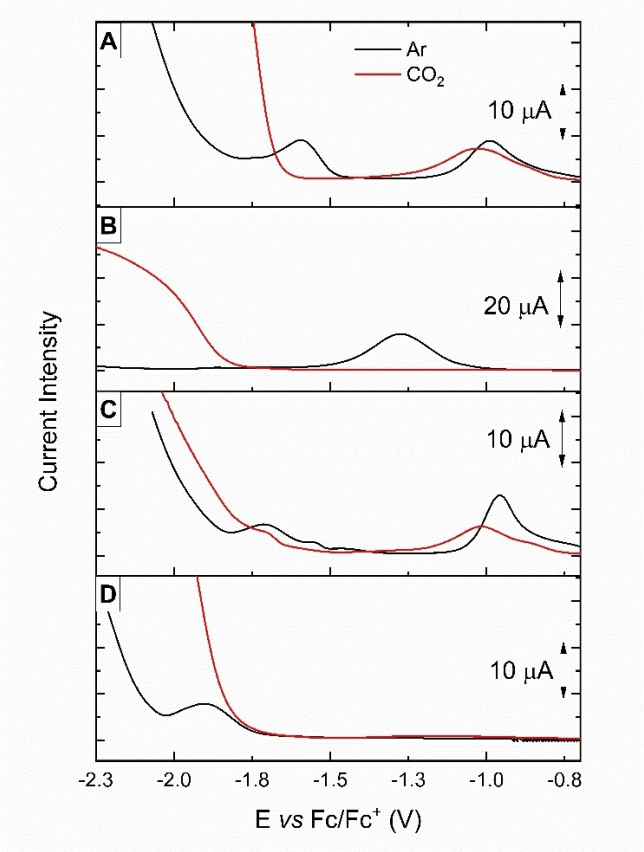

Figure 4. Differential Pulse Voltammetry of **1** (A), **2** (B), **3** (C) and **4** (D) in MeCN/TEOA (5:1, v/v) solution containing 0.1 M $TBAPF_6$ under argon atmosphere (black curves) and CO_2 atmosphere (red curves).

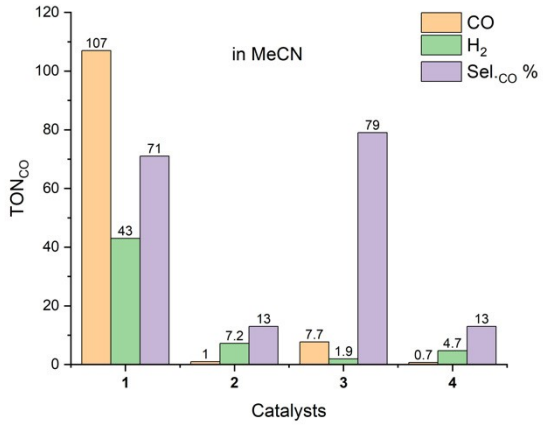

Figure 5. Production and selectivity of CO and H_2 by the catalysts. Amounts of products CO (orange -left column) and H_2 (green – central column) after 4 h of irradiation at 420 nm with 0.1 mM of catalysts **1**, **2**, *3*, and **4** with PS (1.0 mM). The CO selectivity over H_2 in percent is shown in purple (right column).

Table 2. Photocatalytic results comparing **1**, **2**, **3** and **4**.[a]

entry	[CAT][b]	Time	CO/ μmol	H_2/ μmol	TON_{CO}^{CAT}	TON_{H2}^{CAT}	Sel.$_{CO}$[c]
1	Fe-**1**	4 h	37.8	15.1	107	43	71%
2	Fe-**3**	4 h	2.8	0.7	7.8	2	79%
3	Co-**2**	4 h	0.4	2.6	1.1	7.4	13%
4	Co-**4**	4 h	0.2	1.7	0.7	4.9	12%

[a] The experiments were performed in MeCN/TEOA (5:1, v/v) with 20 mM BIH and 1.0 mM PS under CO_2 atmosphere and the products were measured by GC after 4 h irradiation at 420 nm. [b] [CAT] = 0.1 mM [c] Sel.$_{CO}$ = (mol(CO)/(mol(H_2) + mol(CO)))x100.

gaseous contents of the reaction vessel were performed by gas-chromatography, with a chromatograph equipped with two Dielectric-Barrier Discharge Ionization Detectors (BID). The produced amount of CO and H_2 for all complexes are shown in Figure 5 and reported in Table 2.

In acetonitrile, the iron complexes **1** and **3** showed activity towards CO_2, producing carbon monoxide as the main product and molecular hydrogen as a side product, with a selectivity of 71% for **1** and 79% for **3** (Table 2, entries 1–2). In the same conditions, cobalt complexes **2** and **4** produced molecular hydrogen as the main product and only a minor amount of carbon monoxide (Table 2, entries 3–4). The lower activity of the cobalt complexes can be explained by their poor solubility in MeCN. Moreover, their more negative reduction potentials, in comparison to those of the Fe^{II}-based complexes, lead to more basic catalysts and thus more prone to form hydrides, followed by a direct protonation, resulting in competitive H_2 evolution.[25] In this solvent, the efficiency of **1** is very high compared to the other complexes, yielding a TON_{co} of 107 (Table 2, entry 1). Other possible CO_2 reduction products, such as HC(O)OH, CH_3OH, and CH_4, were absent as they could not be detected in the ^1H NMR and GC analyses.

As the heteroleptic Fe-based **1** shows a promising catalytic performance, further optimization of the conditions was explored (Table 3). In particular, different catalyst concentrations were used from 0.01 mM to 0.1mM. Decreasing the concentration of the three components CAT, PS and e-D by a factor of three ([**1**] = 0.033 mM; [PS] = 0.33 mM; [BIH] = 6.6 mM) a higher TON_{CO} of 238 and TON_{H2} of 137 could be achieved (Table 3, entry 3). Nevertheless, increasing the amount of PS and e-D, resulting in a higher ratio of PS/CAT and e-D/CAT ratios, led to an even higher TON_{CO} of 314 and a TON_{H2} of 151 (Table 3, entry 4). The selectivity towards CO remained almost unchanged at an average of 70%. A higher concentration of BIH (100 mM) led to lower efficiency but with the same selectivity (Table 3, entry 6). This phenomenon was already described in similar systems, where a too high concentration of BIH led to a drastic decrease in the activity.[26] A lower concentration of TEOA led to a decrease of activity and a lower selectivity producing CO with a TON of 134 and H_2 with a TON of 110. (Table S8, entry 4).

The best performance was obtained using 0.01 mM of CAT**1**, forming 203 μmol of CO, leading to a TON_{CO} of 576. At the same time, 101 μmol of H_2 were produced (TON_{H2} 287), giving a CO selectivity of 67% after 4 h (Table 3, entry 5). The evolution of CO and H_2 at different concentrations of **1** is shown in Chart

Table 3. Optimization of the photocatalytic reaction with **1** as the catalyst in MeCN/TEOA (5:1).[a]

entry	[CAT]	Time	CO/ µmol	H_2/ µmol	TON_{CO}^{CAT}	TON_{H2}^{CAT}	$Sel._{CO}$
1	**1**	4 h	37.8	15.1	107	43	71%
2	**1**	20 h	38.7	18.9	109	54	67%
3	**1**[b]	4 h	84.1	48.1	238	137	63%
4	**1**[c]	4 h	111	53.0	314	151	67%
5	**1**[d]	4 h	203	101	576	287	67%
6	**1**[e]	4 h	28.2	11.6	80	33	71%
7	**1**[f]	4 h	2.61	2.24	7.4	6.4	54%
8	**1**	1 h	1.1	0.6	3.2	1.6	67%
9	**1**	2 h	28.2	11.9	80	34	70%
10	**1**	3 h	35.4	15.1	100	43	69%
11	**1**[g]	4 h	n.d.	0.3	0	1	–
12	**1**[h]	4 h	n.d.	n.d.	0	0	–
13	**1**[i]	4 h	n.d.	n.d.	0	0	–
14	**1**[j]	4 h	n.d.	n.d.	0	0	–
15	**1**[k]	4 h	32.8	17.5	93	50	65%
16	**1**[l]	4 h	158	122	450	348	56%

[a] The experiments were performed in MeCN/TEOA (5:1, v/v) with 20 mM BIH and 1.0 mM PS under CO_2 atmosphere at 22 °C and the products were measured by GC after 4 h irradiation at 420 nm. The products formed were analyzed from the headspace by GC twice. [b] [CAT] = 0.033 mM, [PS] = 0.33 mM, [BIH] = 6.66 mM. [c] with [CAT] = 0.033 mM, [PS] = 1.0 mM, [BIH] = 20 mM. [d] [CAT] = 0.01 mM, [PS] = 1.0 mM, [BIH] = 20 mM. [e] [BIH] = 100 mM, [f] with 300 uL of H_2O [g] no CAT. [h] no PS. [i] in the dark. [j] no CO_2. [k] In the presence of 1000 equiv. of molecular Hg. [l] With a solar simulator as source of energy, [CAT] = 0.01 mM, [PS] = 1.0 mM, [BIH] = 20 mM, (n.d. = not detected).

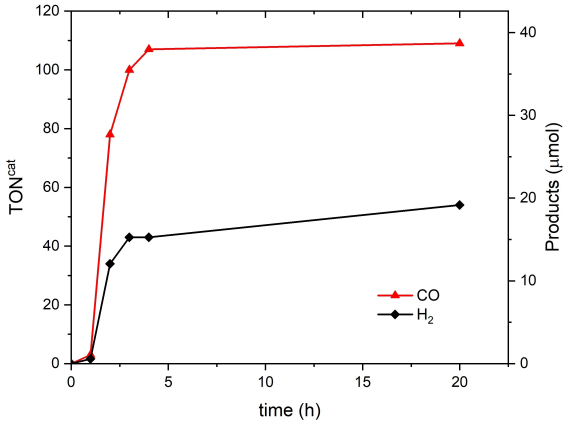

Figure 6. Kinetic studies – Evolution of the production of CO (TON with red curve and quantity in blue) and H_2 (black curve) with the time, using 0.1 mM of **1**, 1.0 mM of PS and 20 mM of BIH in MeCN/TEOA (5:1, v/v) at 420 nm (22 °C).

S1 and reveals the optimum concentration of 0.01 mM. Thus, the performance of CAT **1** is remarkable, when comparing our results to another Fe mononuclear catalyst, Fe-$(dmp)_2(NCS)_2$.[14b,15] The activity of the latter compound was investigated by Ishitani and coworkers in combination with a robust and efficient dinuclear Cu^I complex as a photosensitizer in the same solvent mixture. After 5 hours of irradiation at 436 nm, that system could obtain a TON_{CO} of 95 with coproduction of molecular hydrogen for a CO selectivity of 70.5%.[14b] The increased CO production obtained by extending the irradiation time to 12 h indicated the superior efficiency of the dinuclear Cu^I photosensitizer, reaching a quantum yield of 6.7%. However, when they employed the same Cu^I PS as in our system, Cu^I(dmp)(DPEPhos), the photocatalysis led to a lower TON_{CO} of 69.5 and a CO selectivity of 53%, with a quantum yield of 1.1%.[14b]

In our case, when evaluating the quantum yield of the photocatalytic CO_2 reduction for this system, a value of 7.1% was obtained at 420 nm irradiation for 4 hours. This is amongst the highest quantum yields for homogenous systems based on nonprecious materials.[14b,16a] Kinetic studies show that the photocatalytic system has an induction period of about one hour probably due to the necessary loss of pyridine to access the active catalytic species,[25d,27] and has reached a plateau already after 4 hours of irradiation (Figure 6). In fact, after 20 h, there was no change in the amount of CO, while H_2 production increased slightly, lowering the selectivity for CO from 71% to 67% (Table 3, entry 2). The abrupt ceasing of the catalysis after 4 hours was assumed to be caused by the degradation of the PS. Photostability tests of the catalysts performed by monitoring the UV-vis absorption spectra did not show significant changes (Figure S25). On the contrary, the UV-vis absorption spectra of the photocatalytic solution before irradiation and after 4 h at 420 nm (Figure S24) shows how the metal-to-ligand charge-transfer (MLCT) band of the PS disappeared, denoting the consumption of the heteroleptic Cu^I photosensitizer.

The addition of 0.1 mM water in the solution did not enhance the catalytic activity toward CO production, but it decreased the photocatalytic performance (TON_{CO} 7.4 and TON_{H2} 6.4, Table 3, entry 7).

Control experiments were carried out to prove that each component of the photocatalytic system herein presented is necessary for the photoinduced reduction of carbon dioxide. When tests were conducted under an Ar atmosphere, in the dark, or without PS, no production of CO or H_2 could be detected (Table 3, entries 12, 13, 14). Even if BIH constitute the main source of electrons, TEOA can also act as a proton donor.[28] It is in fact demonstrated by the entry 3 in Table 3 where the sum of the TON values ($TON_{H2} + TON_{CO}$) exceeds the molar ratio BIH/CAT while both H_2 and CO are 2 electrons processes. A control test without BIH (Table S8, entry 1) show the production of CO with a TON of 6.8 proving the low but positive electron-donating ability of TEOA. Interestingly, without BIH the selectivity for CO over H_2 exceeds 99% as no H_2 could be observed. In a further control test without TEOA, the production of 1.73 µL of CO (TON_{CO} 44) (Table S8, entry 2) and also in this case no production of H_2. The system with only BIH gave a lower production of CO in comparison to the optimized system maybe because the cationic radical of BIH after the first reduction of PS* could not be easily deprotonated in absence of TEOA. Nevertheless, we detected the formation of methane. These interesting findings deserve a closer study that is ongoing.

When CAT **1** was absent, no CO was formed; however, traces of H_2 were detected (0.4 µmol, $TON_{H2} = 1$) (Table 3, entry 11), indicating that the PS contributes to the formation of H_2. The homogeneity of the active catalyst was tested by

dynamic light scattering (DLS) experiments (Figure S28, S29) of the photocatalytic solutions. Small amounts of nanoparticles with an average size of 100 nm were found before and after irradiation. This result indicates that they are not formed during the photoreaction. In addition, a peak for 1 nm-sized nanoparticles was found after irradiation with a negligible intensity. To prove that the catalysis occurs by the dissolved components, a mercury test was performed, by adding 1000 equivalents of molecular Hg in the sample with vigorous agitation, in order to remove potential metallic nanoparticles. No significant change was observed in the production of CO and H_2 (Table 3, entry 15). Thus, both experiments allow us to assume the homogeneity of the catalytic solution.

In order to check the feasibility of the photocatalytic CO_2 reduction with our system under sunlight, a solar simulator was employed as source of energy. The photocatalytic systems contained 0.01 mM of **1** with 1.0 mM of PS and showed production of CO and H_2 with TONco = 450 and TON_{H2} = 348 after 4 h. (Table 3, entry 16). The CO selectivity dropped to 56 %. The lower selectivity obtained can be explained by a faster decomposition of the PS under white light, forming the lower-performing homoleptic $Cu^{I}(dmp)_2$ as seen by its characteristic metal-to-ligand charge transfer (MLCT) absorption band at 460 nm (Figure S26).[29] The formation of the not active homoleptic $Cu^{I}(dmp)_2$ was also proved by ^{1}H NMR (Figure S27) after irradiation. The quantum efficiency of the photocatalytic system was calculated, measuring the irradiated light intensity by chemical actinometry (see the experimental part for details). For the system using **1** as CAT, the quantum yield is evaluated after 4 h Φ = 4.5 % with the white light of the solar simulator.

Experiments using the ^{13}C isotope were conducted to confirm the origin of CO coming from CO_2 (Figure 7). Three typical photocatalytic tests were prepared in NMR tubes provided with a J. Young valve. Two of them under a $^{13}CO_2$ atmosphere, and the third one under $^{12}CO_2$ atmosphere. The first sample under a $^{13}CO_2$ atmosphere contains **1** as CAT (Figure 7 top) and the second one contains no CAT (Figure 7 bottom). The sample under a $^{12}CO_2$ atmosphere contains **1** as CAT (Figure S31, C).

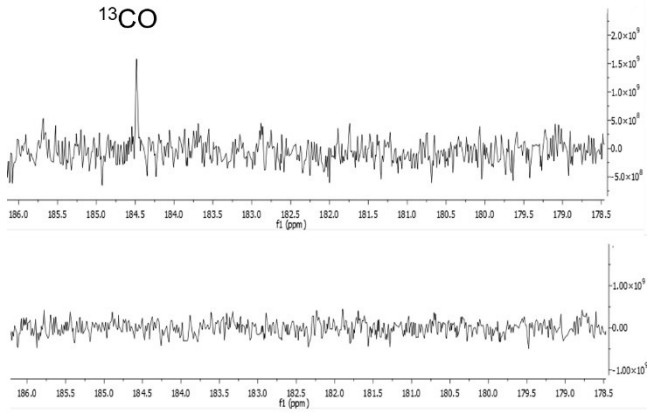

Figure 7. ^{13}C NMR of a typical photocatalyst test under a $^{13}CO_2$ atmosphere with **1** as CAT (top) and without CAT (bottom).

The ^{13}C NMR spectrum of the first test under $^{13}CO_2$ atmosphere with CAT shows a signal for the carbon of the produced and dissolved CO at 184 ppm.[30] This signal is not observed in the test containing no catalyst (Figure 7, bottom). This signal is also not observed in the spectrum of the sample under $^{12}CO_2$ atmosphere. This indicates that the CO produced can only be due to the photoreduction of CO_2 by **1**.

In order to determine which quenching mechanism applies to the excited photosensitizer PS*, bimolecular Stern-Volmer (SV) quenching analyses were performed in the same solvent used for the photocatalytic reactions MeCN/TEOA (5:1, v/v). Both a reductive quenching by BIH and oxidative quenching by CAT **1** are thermodynamically feasible with quenching constants $k_{BIH} = 0.10 \times 10^6\ s^{-1}\,m^{-1}$ and $k_{CAT} = 0.2 \times 10^6\ s^{-1}\,m^{-1}$. These quenching constants are lower than those reported in the literature using Cu(dmp)DPEPhos as the PS and BIH as the electron donor, probably as a result of measuring in the MeCN/TEOA mixture rather than only in MeCN. Despite the higher values of the constant for the oxidative quenching, the reductive quenching by BIH is favored because of the significantly higher concentration of BIH in the solution compared with the concentration of CAT ([BIH] = 20 mM $\gg$ [CAT] = 0.1 mM). Thus, photoinduced electron transfer from BIH to PS* occurs, and the reduced form of PS is oxidized back by the catalyst. The linear responses of the SV experiments are given in the Supporting information, Figures S22 and S23. As already known in the literature, also the radical $BI^{\bullet}$ is a very good reductant ($E_{ox} = -2.06$ vs Fc^+/Fc).[31] However, the driving force of the electron transfer towards PS* is almost zero (ΔG = 0.02 eV, Eq. S3 in ESI). Thus, it is unlikely that $BI^{\bullet}$ reduces PS*.

Computational Studies

Computational studies were conducted on CAT **1** to get insight into the catalytic cycle for CO_2 reduction. For comparison calculations were also performed on the iron-based homoleptic analogue **3**, as they are the complexes that produced mainly CO from CO_2.

To confirm that the thiocyanates ligands are binding the metal through the nitrogen, different linkage isomerism (due to ambidentate ligand) were investigated with different spin states for complex **1**.[32] As expected from the precursor NH_4NCS employed, independently from the spin state, the N-bonded thiocyanate complex is energetically preferred to the S-bonded. The lowest energy was found for the triplet state, with a quintet state only slightly higher in energy (Table S13). The Mulliken spin populations for different multiplicities are given in the supporting information, (Figure S40). Quintet and triplet differ by the coupling of the Fe and the ligand spin and are very similar in energy. Therefore, the quintet state is omitted in the following. Mulliken population analyses were conducted on both complexes, and the spin density plots are shown in Figure S34 and Table S10. When reduced, the additional electrons partly go to the ligand(s) for both complexes. Moreover, with adsorption of CO_2, the unpaired electrons are mainly localized on the iron centers and to a lower extent on the

adsorbed CO_2 as well as the ligand system. (Table S13 and Figure S39)

In electrochemical processes, the charge of the catalytic complex can easily change. Concerning CO_2 reduction, it is known that CO_2 can be adsorbed only on reduced metals for similar types of complexes.[33] First, the energetics of charge changes of both complexes were studied (Figure S32). Therefore, we discuss the total charge of the complexes.

In complex **1**, the pyridine is the weakest ligand, as its binding energy to Fe^{2+} in the neutral $FeL(NCS)_2py$ was calculated to be 52.56 kJ/mol while the binding energy of NCS is much stronger (596.46 kJ/mol). The thermodynamics of ligand dissociation and CO_2 adsorption on both complexes with different charge states were then investigated (Figure S34, S35).

In agreement with literature data,[34] it was found that even when coordination on the metal center is geometrically allowed, CO_2 is only stable with two times reduced complexes. (Figure S36). Moreover, CO_2 adsorption is only possible for all the complexes after the release of a coordinated ligand to maintain the octahedral conformation. In the case of complex **3**, one of the triazole rings is released to render the accessibility of the Fe center. For this transformation, less energy (17 kJ/mol) is required. (Figure S35)

Furthermore, the adsorption of CO_2 on the iron centers of **1** and **3** was investigated. CO_2 can be adsorbed on the metal centers in different ways, and the four most common, namely linear-O-"end-on" (η^1 **o**), "side-on" (η^2 **c**, **o**), C-bound "Y-on" (η^1 **c**) and O-bent "end-on" (η^1 **o** ***bent***) were tested (Figure 8).[35]

The C-bound (η^1 **c**) "Y-on" configuration was found the most stable in a singlet state for complex **1** while CO_2 binds most preferably "side-on" (η^2 **c**, **o**) in a triplet state in complex **3** (Table S12).

The proposed mechanism of CO_2 reduction with **1** as catalyst is shown on Scheme 1. The first step consists of the loss of the pyridine to reach the complex A^0. In the next step, A^0 is photo- inductive reduced by two PS^- to A^{2-} enabling CO_2 adsorption in "Y-on" conformation. The CO_2-complex B^{2-} formed is then doubly protonated to form the complex C^0.[36] The weaker C–O bond can then break to free a molecule of water by overcoming the barrier of 160 kJ/mol in the singlet state (200 + kJ/mol for the triplet state), reaching D^0. The desorption of CO as the last step was investigated, and the detachment energies are given in Table 4.

This step is crucial because the CO-metal bond can be very stable,[37] causing overstabilization of this complex and thus, degradation of the active catalyst, limiting the reaction.

For complex **1**, CO is released from the iron center to recover A^0 using 137 kJ/mol (Table 4).

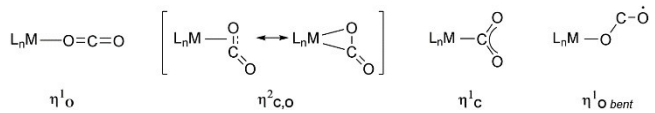

Figure 8. Mode of coordination of CO_2.

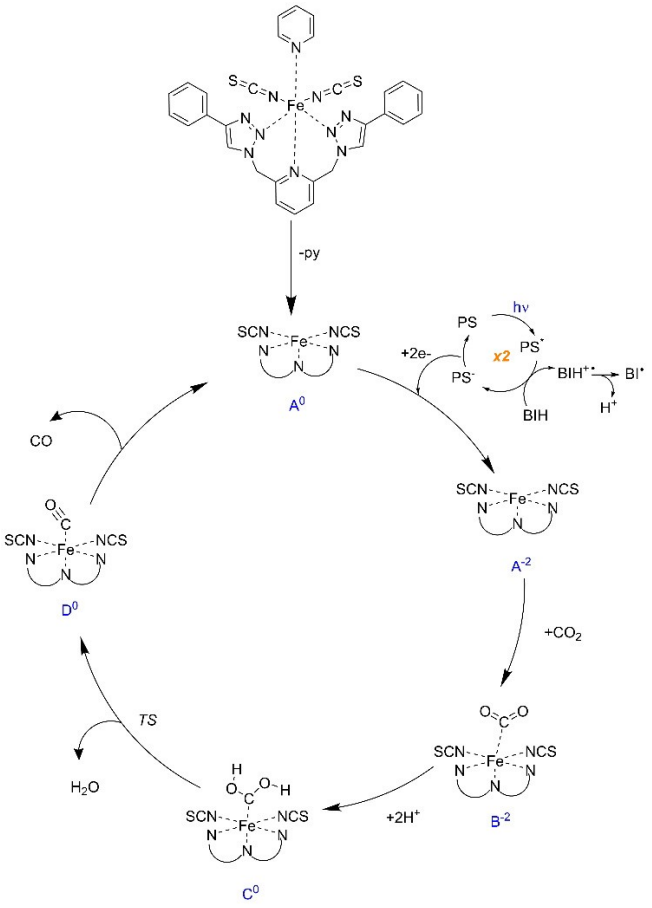

Scheme 1. Proposed mechanism for the photocatalytic CO_2 reduction with **1**.

Table 4. Desorption energies for CO from CAT **1** and **3**.

	CAT **1** (0, 1) [kJ/mol]	CAT **3** (0, 1) [kJ/mol]
Electronic energy	197.61	182.75
Thermal energy (ZPE)	187.44	168.82
Gibbs free energy	137.74	120.79

The reaction profiles obtained for **1** in different multiplicities are shown in Figure 9. The most favourable pathway is found to be in the singlet state, showing the lowest barriers. The most energy-demanding step is the proton transfer to form coordinated water (160 kJ/mol). The release of CO makes the reaction exothermic (−40 kJ/mol).

Scheme 2 shows a similar mechanism for the reduction of CO_2 with **3** as the catalyst. Because of the neutral charge of the ligands, the charge of the different intermediates in the reaction with complex **3** is always higher (by 2 positive charges) compared to complex **1**. The precursor **3** has a charge of 2+ that is reduced by the uptake of two electrons opening the ligand to form A^0. Since the active center of **3** is more hindered in comparison to that of **1**, the adsorption of CO_2 is expected to be less probable. Even with slightly lower energy gained by the ligand-to-CO_2 exchange at the most reduced state, the equili-

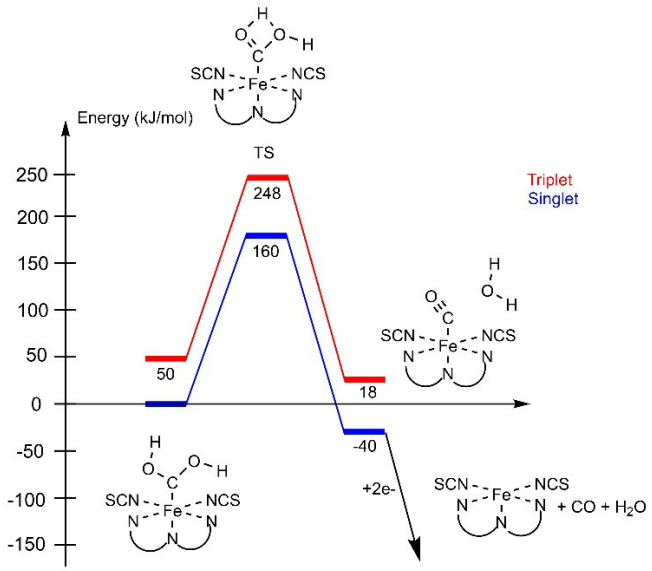

Figure 9. Energy diagram for CAT **1** in different multiplicities.

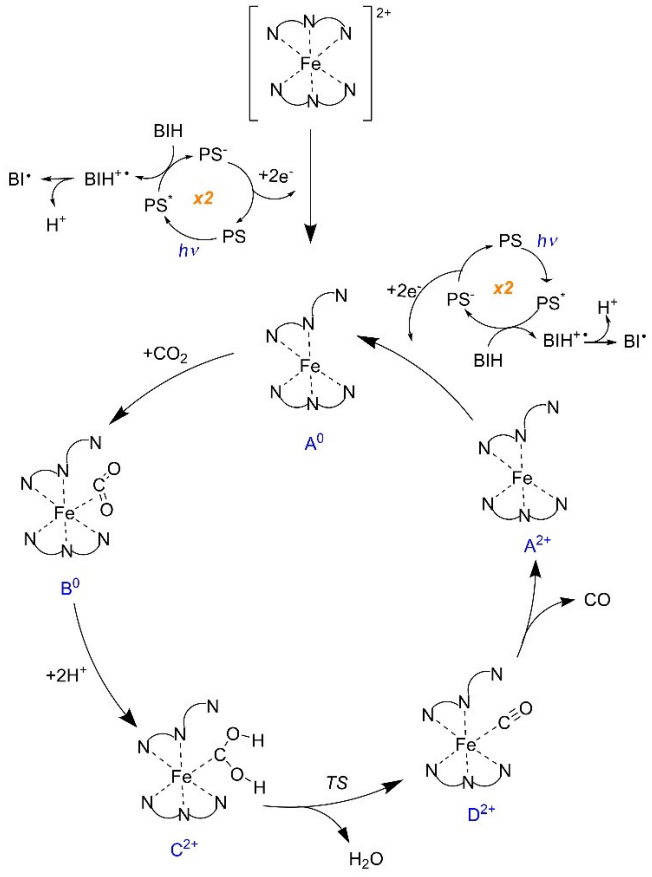

Scheme 2. Proposed mechanism for the photocatalytic CO_2 reduction with **3**.

brium in the reaction conditions might be significantly shifted to "closed" unreactive forms. Contrary to complex **1** where CO_2 binds "Y-on" "(η^1 **c**), CO_2 binds "side-on" (η^2 **c**, **o**) to the metal center. Finally, the catalytic cycle involving **3** follows the same last steps as for complex **1**. Similar to the mechanism involving **1**, the last step, which is the releasing of CO, needs 120 kJ/mol to regenerate A^0 (Table 4). The desorption of CO is slightly easier with **3** because of the sterically hindered structure of the molecule.

The reaction profiles obtained for **3** in different multiplicities are shown in Figure 10. As for **1**, the protonation pathway is more favourable in the singlet state with the lowest barriers. The most energy demanding step is also in this case, the proton transfer to form coordinated water (165 kJ/mol). The release of CO makes the reaction exothermic but releases less energy than with **1** (−20 kJ/mol).

For complex **3** a second pathway has been investigated involving simultaneous proton and electron transfers.[33b,38] The charge of the complex remains unchanged during the whole cycle. (Figure S37). The energies of the transition states (TS) and of the intermediates in Schemes 1 and 2 for different spin states are shown in Figures 9 and 10 and their electronic and relative energies are shown in Table S9. The quintet states were omitted because of their approximately 40 kJ/mol higher energies than the singlet states for C and D.

To verify experimentally that the first step of the catalytic mechanism with **1** is the loss of the pyridine, NanoESI of a sample containing **1** in MeCN was performed (Figures S4 and S5). It shows a mass of 507.080 for the fragment [**1** – NCS – pyridine] and a mass of 585.094 for the fragment [**1** – NCS], indicating that the pyridine can stay coordinated to Fe when dissolved only in MeCN (Figure S5). The evidence of reaction between the metallic centre of the catalyst and TEOA has been demonstrated in several systems.[39] TEOA can participate in the capture of CO_2 by easy insertion in the metal – O(TEOA) bond. Concerning our system, NanoESI of a sample containing one equivalent of **1** withtwo equivalents of TEOA in MeCN shows a

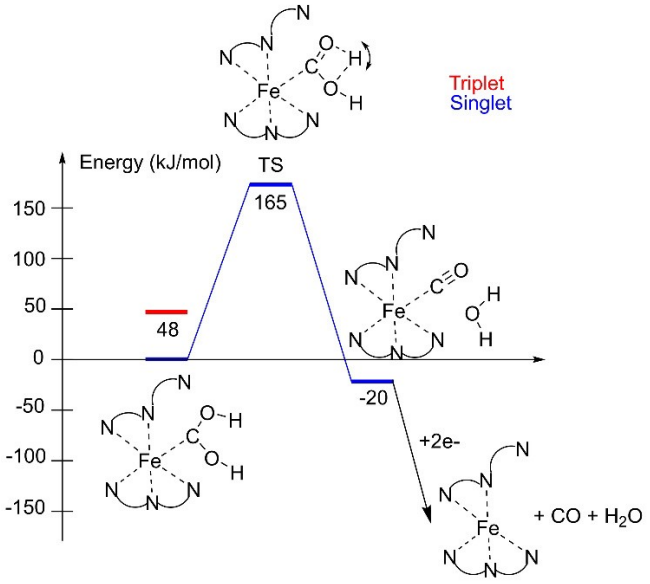

Figure 10. Energy diagram for CAT **3** for different multiplicities.

mass of 655.633 for [1−Py+TEOA], revealing that the pyridine can be replaced by TEOA (Figure S6). Further experiments and analysis would be needed to determine if and how such an adduct would play a role in the reduction of CO_2.

Conclusion

In summary, this work reports the synthesis and full characterization of a new iron heteroleptic complex based on the N,N,N-pincer ligand 2,6-bis(4′-phenyl-1′,2′,3′-triazol-1-yl-methyl)pyridine. We have shown the high activity of this new catalyst in the photo-driven reduction of carbon dioxide, in combination with a heteroleptic copper complex, acting as a photosensitizer under visible light. We compared its activity to its cobalt analogue and the corresponding homoleptic iron- and cobalt-based complexes, revealing that in MeCN the iron complexes are remarkably more effective than the cobalt analogues. Using DFT methods, we identified transition states and estimated reaction barriers, distinguished possible mechanisms and stabilities of potentially involved intermediates, *i.e.*, CO-dissociation energy. Our fully earth-abundant system with the heteroleptic Fe^{II}-complex **1** converted CO_2 into carbon monoxide with a TON_{CO} up to 576 after 4 h of irradiation at 420 nm. The apparent quantum yield for this system was calculated to be 7.1 %. The activity of **1** is among the highest reported using monometallic iron-based catalysts in a complete earth-abundant system. Furthermore, the coproduction of molecular hydrogen prompts further investigations of this system to produce syngas from CO_2 under solar light.

Experimental Section

General information. All solvents were purchased from Sigma Aldrich and distilled several times over-drying agents before use. BIH was synthesized as previously described[28a] and recrystallized three times before use. DMP, DPEPhos, metal precursors and other chemicals were purchased from Sigma Aldrich, ABCR, and were used as received. ^1H and ^{13}C NMR spectra were acquired on a Brucker Avance 400 MHz spectrometer. Electron Spray Ionization mass (ESI) spectra were recorded on a Thermo Scientific Q Exactive Plus mass spectrometer in positive ion mode and NanoESI was recorded on a LTQ-Orbitrap XL from ThermoFisher Scientific with a home-built NanoESI source.

Synthesis. To form the paramagnetic complexes **1** and **2**, a solution of L (1.00 equiv.) in MeOH was added to a solution of $M(SCN)_2py_4$ (1.00 equiv.) in MeOH. The colour of the solution changed instantly and the mixture was stirred at 20 °C for 40 min. The solvent was removed under vacuum in rotary evaporator and the powder obtained was washed three times with methanol and diethyl ether. The powder was recrystallized with MeCN and diethyl ether. The desired product was obtained as a coloured powder with 60 %, 79 % of yield for **1**, and **2** respectively.

EA Anal. Calc. for **1** + diethyl ether + pyridine $C_{30}H_{24}FeN_{10}S_2 + C_4H_{10}O + C_5H_5N$: N, 19.31, C, 58.72, H, 4.29, S, 8.74, Found: N, 18.7, C, 58.11, H, 4.42, S, 8.74. NanoESI-MS (m/z): 507.080 [M−SCN−py], 585.094 [M−NCS].

EA Anal. Calc. for **2** $C_{30}H_{24}CoN_{10}S_2$: N, 21.63, C, 55.64, H, 3.74, S, 9.90 Found: N, 19.8, C, 55.8, H, 3.75, S, 9.15. ESI-MS (m/z): 510.2 [M−NCS−py].

Deposition Numbers 2173070 (1), 2173071 (2) contain the supplementary crystallographic data for this paper. These data are provided free of charge by the joint Cambridge Crystallographic Data Centre and Fachinformationszentrum Karlsruhe Access Structures service.

The diamagnetic complex **3** and paramagnetic complex **4** were synthesized according to the literature procedures.[19] A solution of L (2.00 equiv.) in MeOH was added to a solution of $M(ClO_4)_2$, $\bullet H_2O$ (1.00 equiv.) in MeOH. The colour of the solution changed instantly and the mixture was stirred at room temperature for 40 min. The solvent was removed under vacuum and the powder obtained was washed three times with cold methanol and diethyl ether. The desired product was obtained as a coloured powder with 95 % and 89 % of yield for **3** and **4** respectively.

Complex **3**: ^1H NMR (400 MHz, MeCN d_3): 9.46 (s, 2H), 8.89 (s, 4H), 8.32 (t, 2H), 7.86 (t,5H), 7.29 (m,21H), 5.72 (m, 4H). EA Anal. Calc. for **3** $C_{46}H_{38}ClFeN_{14}O_4$−: N, 20.81, C, 58.64, H, 4.07, Found: N, 21.17, C, 59.88, H, 4.40. ESI-MS (m/z): 941.3 [M−(ClO_4)]

EA Anal. Calc. for **4** $C_{46}H_{38}ClCoN_{14}O_4$: N, 18.77, C, 52.88, H, 3.67, Found: N, 18.9, C, 53.6, H, 3.53. ESI-MS (m/z): 944.2 [M−(ClO4)]

Electrochemistry. Cyclic voltammetry and differential pulse voltammetry were recorded on a Gamry Interface 1010B using a 3 electrodes cell system. The working electrode was a glassy carbon, the auxiliary electrode a Pt wire and the quasi-reference electrode an Ag wire; thus, ferrocene was used as the internal standard. All experiments were conducted in a MeCN/TEOA (5 : 1, v/v) with 0.1 M $TBAPF_6$ as supporting electrolyte under argon or CO_2 atmosphere. For easier comparison, according to IUPAC recommendation, all the redox properties were reported versus ferrocene (Fc^+/Fc couple).

Photophysics. UV/vis absorption spectra were recorded in MeCN with ALS SEC 2020 Wide wavelength range spectrometer (200–1025 nm). Emission spectra were recorded with a Fluoromax 4 from Horiba Jobin.

Photocatalytic experiments. The photocatalytic tests were conducted in a similar way than previously.[8d] They contain (unless otherwise specified) 4.0 mL of a MeCN/TEOA (5 : 1 v/v) solution containing CAT (0.01 to 0.1 mM), PS1 (1.0 mM), BIH (20 mM). CO_2 (purity $\geq$ 99.995 %) is then bubbled through the solution for 12 min prior to initiate the photolysis. The tests were then irradiated at 420 nm in a photoreactor LZC-IC2 from Luzchem with 2 fluorescent lamps (8 W). The temperature was constant at 22 °C. Actinometry using $K_3Fe(C_2O_4)_3$ was performed to determine the total photon flux (2.5×10^{-8} E s^{-1}) and the number incident photons. The quantum yields for CO (Φ_{CO}) and H_2 (Φ_{H2}) formations were calculated using the following equation:

$$\Phi(\%) = \frac{2 * number\ of\ molecules}{number\ of\ photon\ absorbed * fap} * 100$$

f_{ap} represents the fraction of absorbed photons by the photocatalytic test at 420 nm ($1\text{-}10^{-A}$). Factor 2 conveys the electrons needed to reduce CO_2 into CO. The number of molecules CO formed was determined by quantitative GC measurement (Shimadzu GC-2030) from the headspace of the reaction, using Shimadzu BID-2030 detectors, column 1 Shimadzu SH-Rt-U-Bond PLOT; 0.32 mm ID; 10 um df; 30 m, column 2 Shimadzu SH-Rt-Msieve 5 Å; 0.32 mm ID; 30 μm; 30 m, and Ar as carrier gas. 50 μL of gas were automatically injected (AOC-6000 plus RSI LIQUID HS) with a gas-tight syringe and a split injection of 1/20. The method description

is: incubation of sample at 30 °C for 5 min, injection 50 μL, 20 split ratio, at oven temp. 40 °C, 2 min after injection begin ramping over 7 min to 180 °C, hold 180 for 2 min., col.1 flow 3.32 ml/min, col.2 flow 1.85 ml/min. Calibration curves were carried out with known standard quantities of CO and H_2. The experiments were conducted at least twice (error $< 15\,\%$).

Mercury poisoning tests. A large excess of molecular mercury (1000 equiv.) was added in a typical catalytic test (4 mL) with 1 (0.1 mM) as catalyst under CO_2 atmosphere, and vigorously stirred all along the 4 hours irradiation at 420 nm. Mercury poisoning test consists of removing possible heterogeneous metal nanoparticles if and when formed after decomposition of 1 and PS. It is an indication and not a proof to determine the presence or lack of heterogeneous materials in our photolysis solutions.

Carbon-13 labelling experiments. The solutions (4 mL) containing or not **1** (0.1 mM), PS (1 mM), BIH (20 mM) was purged with Ar for 10 min, followed by $^{13}CO_2$ previously formed by adding H_2SO_4 conc. on $NaH^{13}CO_3$ (purchased from Sigma Aldrich). The ^{13}CO generated during the photoirradiation was detected by ^{13}C NMR.

Quantum chemical calculations. The calculations of the CO_2 binding energies were performed with the program package Turbomole[40,41] using density functional theory (DFT) with the B3LYP functional[34a] and a def2-TZVP basis set.[34b,c] For the determination of reaction mechanisms the r^{2}SCAN-3c method,[42] which includes D4-dispersion[43] as well as the geometrical Counterpoise Correction (gCP)[44] and a modified version of the def2-TZVP basis set is used.[45] The r^{2}SCAN calculations were performed with ORCA 5.0.2.[46]

Acknowledgements

We are grateful for the financial support by the German Research Foundation (DFG) transregional collaborative research center SFB/TRR 88 "Cooperative Effects in Homo and Heterometallic Complexes (3MET)" (projects B9, B1 and A5). C. B. thanks the Young Investigator Network (YIN) of KIT for providing additional financial support through the YIN Award. E.B and K.F. acknowledge support by the state of Baden-Württemberg through bwHPC and the DFG through grant no INST 40/575-1 FUGG (JUSTUS 2 cluster). Dr. N. Jung and Dr. P. Hodapp are acknowledged for giving access to the GC and Dr. P. Weis and Dr. M. Neumaier for the NanoESI experiments. DLS experiments were performed with the help of F. Ferrari. Open Access funding enabled and organized by Projekt DEAL.

Conflict of Interest

The authors declare no conflict of interest.

Data Availability Statement

The data that support the findings of this study are available in the supplementary material of this article.

Keywords: carbon dioxide reduction · earth-abundant materials · iron complexes · noble-metal free artificial photosynthesis · syngas

[1] in Forest absorb twice as much carbon as they emit each year, Vol. **2021**. https://www.wri.org/insights/forests-absorb-twice-much-carbon-they-emit-each-year.
[2] a) D. Gust, in *Chapter One – An Illustrative History of Artificial Photosynthesis, Vol. 79* (Ed.: B. Robert), Academic Press, **2016**, pp. 1–42; b) G. Centi, S. Perathoner, *ChemSusChem* **2010**, *3*, 195–208; c) D. R. Whang, D. H. Apaydin, *ChemPhotoChem* **2018**, *2*, 148–160; d) N. Roy, N. Suzuki, C. Terashima, A. Fujishima, *Bull. Chem. Soc. Jpn.* **2019**, *92*, 178–192.
[3] a) in *The carbon cycle*, *Vol.* **2019**; https://www.elsevier.com/books/the-global-carbon-cycle-and-climate-change/reichle/978-0-12-820244-9; b) H. Dau, E. Fujita, L. Sun, *ChemSusChem* **2017**, *10*, 4228–4235; c) B. Zhang, L. Sun, *Chem. Soc. Rev.* **2019**, *48*, 2216–2264.
[4] E. Fujita, *Coord. Chem. Rev.* **1999**, *185–186*, 373–384.
[5] a) D. S. Laitar, P. Müller, J. P. Sadighi, *J. Am. Chem. Soc.* **2005**, *127*, 17196–17197; b) C.-F. Leung, T.-C. Lau, *Energy Fuels* **2021**, *35*, 18888–18899.
[6] a) N. W. Kinzel, C. Werlé, W. Leitner, *Angew. Chem. Int. Ed.* **2021**, *60*, 11628–11686; b) C. Jiang, A. W. Nichols, C. W. Machan, *Dalton Trans.* **2019**, *48*, 9454–9468.
[7] a) H. Takeda, H. Kamiyama, K. Okamoto, M. Irimajiri, T. Mizutani, K. Koike, A. Sekine, O. Ishitani, *J. Am. Chem. Soc.* **2018**, *140*, 17241–17254; b) L. Chen, Y. Qin, G. Chen, M. Li, L. Cai, Y. Qiu, H. Fan, M. Robert, T.-C. Lau, *Dalton Trans.* **2019**, *48*, 9596–9602; c) M. Feller, U. Gellrich, A. Anaby, Y. Diskin-Posner, D. Milstein, *J. Am. Chem. Soc.* **2016**, *138*, 6445–6454; d) M. Vogt, A. Nerush, Y. Diskin-Posner, Y. Ben-David, D. Milstein, *Chem. Sci.* **2014**, *5*, 2043; e) R. Bonetto, R. Altieri, M. Tagliapietra, A. Barbon, M. Bonchio, M. Robert, A. Sartorel, *ChemSusChem* **2020**, *13*, 4111–4120; f) M. Isaacs, J. C. Canales, M. J. Aguirre, G. Estiú, F. Caruso, G. Ferraudi, J. Costamagna, *Inorg. Chim. Acta* **2002**, *339*, 224–232; g) J. Grodkowski, P. Neta, E. Fujita, A. Mahammed, L. Simkhovich, Z. Gross, *J. Chem. Phys. A* **2002**, *106*, 4772–4778; h) A. J. Morris, G. J. Meyer, E. Fujita, *Acc. Chem. Res.* **2009**, *42*, 1983–1994; i) S. L.-F. Chan, T. L. Lam, C. Yang, S.-C. Yan, N. M. Cheng, *Chem. Commun.* **2015**, *51*, 7799–7801; j) L. Chen, Z. Guo, X.-G. Wei, C. Gallenkamp, J. Bonin, E. Anxolabéhère-Mallart, K.-C. Lau, T.-C. Lau, M. Robert, *J. Am. Chem. Soc.* **2015**, *137*, 10918–10921; k) J. Bonin, M. Chaussemier, M. Robert, M. Routier, *ChemCatChem* **2014**, *6*, 3200–3207; l) P. G. Alsabeh, A. Rosas-Hernández, E. Barsch, H. Junge, R. Ludwig, M. Beller, *Catal. Sci. Technol.* **2016**, *6*, 3623–3630.
[8] a) C. D. Windle, R. N. Perutz, *Coord. Chem. Rev.* **2012**, *256*, 2562–2570; b) S. K. Lee, M. Kondo, M. Okamura, T. Enomoto, G. Nakamura, S. Masaoka, *J. Am. Chem. Soc.* **2018**, *140*, 16899–16903; c) M. H. Rønne, D. Cho, M. R. Madsen, J. B. Jakobsen, S. Eom, É. Escoudé, H. C. D. Hammershøj, D. U. Nielsen, S. U. Pedersen, M.-H. Baik, T. Skrydstrup, K. Daasbjerg, *J. Am. Chem. Soc.* **2020**, *142*, 4265–4275; d) L.-L. Gracia, L. Luci, C. Bruschi, L. Sambri, P. Weis, O. Fuhr, C. Bizzarri, *Chem. Eur. J.* **2020**, *26*, 9929–9937.
[9] D. K. Chauhan, N. Sharma, K. Kailasam, *Mater. Adv.* **2022**, *3*, 5274–5298.
[10] C. Ghenai, Advances, in *Mechanical Engineering* **2010**, *2*, 342357.
[11] S. R. Foit, I. C. Vinke, L. G. J. de Haart, R.-A. Eichel, *Angew. Chem. Int. Ed.* **2017**, *56*, 5402–5411; *Angew. Chem.* **2017**, *129*, 5488–5498.
[12] a) H. Rao, J. Bonin, M. Robert, *ChemSusChem* **2017**, *10*, 4447–4450; b) X. Zhang, M. Cibian, A. Call, K. Yamauchi, K. Sakai, *ACS Catal.* **2019**, *9*, 11263–11273; c) D. Dedić, A. Dorniak, U. Rinner, W. Schöfberger, *Front. Chem.* **2021**, *9*; d) X. Zhang, K. Yamauchi, K. Sakai, *ACS Catal.* **2021**, *11*, 10436–10449; e) H. Yuan, B. Cheng, J. Lei, L. Jiang, Z. Han, *Nat. Commun.* **2021**, *12*, 1835; f) H. Rao, C.-H. Lim, J. Bonin, G. M. Miyake, M. Robert, *J. Am. Chem. Soc.* **2018**, *140*, 17830–17834; g) L. Zou, R. Sa, H. Lv, H. Zhong, R. Wang, *ChemSusChem* **2020**, *13*, 6124–6140; h) K. Guo, X. Li, H. Lei, H. Guo, X. Jin, X.-P. Zhang, W. Zhang, U.-P. Apfel, R. Cao, *Angew. Chem. Int. Ed.* **2022**, *61*, e202209602; i) Y. Wang, X.-P. Zhang, H. Lei, K. Guo, G. Xu, L. Xie, X. Li, W. Zhang, U.-P. Apfel, R. Cao, *CCS* **2022**, *4*, 2959–2967; j) R. Cao, *ChemSusChem* **2022**, *15*, *e202201788* n/a, https://doi.org/10.1002/cssc.202201788
[13] a) Y. Wang, T. Liu, L. Chen, D. Chao, *Inorg. Chem.* **2021**, *60*, 5590–5597; b) Z. Guo, G. Chen, C. Cometto, B. Ma, H. Zhao, T. Groizard, L. Chen, H. Fan, W.-L. Man, S.-M. Yiu, K.-C. Lau, T.-C. Lau, M. Robert, *Nat. Catal.* **2019**, *2*, 801–808; c) Z. Guo, S. Cheng, C. Cometto, E. Anxolabéhère-Mallart, S.-M. Ng, C.-C. Ko, G. Liu, L. Chen, M. Robert, T.-C. Lau, *J. Am. Chem. Soc.* **2016**, *138*, 9413–9416; d) Y. Qin, L. Chen, G. Chen, Z. Guo, L. Wang, H.

Fan, M. Robert, T.-C. Lau, *Chem. Commun.* **2020**, *56*, 6249–6252; e) M. Loipersberger, D. G. A. Cabral, D. B. K. Chu, M. Head-Gordon, *J. Am. Chem. Soc.* **2021**, *143*, 744–763.
[14] a) A. Rosas-Hernández, C. Steinlechner, H. Junge, M. Beller, *Green Chem.* **2017**, *19*, 2356–2360; b) H. Takeda, K. Ohashi, A. Sekine, O. Ishitani, *J. Am. Chem. Soc.* **2016**, *138*, 4354–4357.
[15] H. Takeda, Y. Monma, O. Ishitani, *ACS Catal.* **2021**, *11*, 11973–11984.
[16] a) C. Bizzarri, *Eur. J. Org. Chem.* **2022**; C. Bizzarri, *Eur. J. Org. Chem.* **2022, e202200185** b) K. E. Dalle, J. Warnan, J. J. Leung, B. Reuillard, I. S. Karmel, E. Reisner, *Chem. Rev.* **2019**, *119*, 2752–2875; c) H. Takeda, C. Cometto, O. Ishitani, M. Robert, *ACS Catal.* **2017**, *7*, 70–88; d) A. Rosas-Hernández, C. Steinlechner, H. Junge, M. Beller, *Top. Curr. Chem.* **2017**, *376*, 1; e) H. Chen, L. Chen, G. Chen, M. Robert, T.-C. Lau, *ChemPhysChem* **2021**, *22*, 1835–1843; f) Y. Wang, X.-W. Gao, J. Li, D. Chao, *Chem. Commun.* **2020**, *56*, 12170–12173; g) E. Boutin, L. Merakeb, B. Ma, B. Boudy, M. Wang, J. Bonin, E. Anxolabéhère-Mallart, M. Robert, *Chem. Soc. Rev.* **2020**, *49*, 5772–5809.
[17] in Handbook of Chemistry and physics – Abundance of elements in the earth's crust and in the sea, https://hbcp.chemnetbase.com/faces/documents/14 10/14 10 0001.xhtml .
[18] D. G. Cuttell, S.-M. Kuang, P. E. Fanwick, D. R. McMillin, R. A. Walton, *J. Am. Chem. Soc.* **2002**, *124*, 6–7.
[19] W. S. Brotherton, P. M. Guha, H. Phan, R. J. Clark, M. Shatruk, L. Zhu, *Dalton Trans.* **2011**, *40*, 3655–3665.
[20] S. Mahapatra, R. J. Butcher, R. Mukherjee, *Dalton Trans.* **1993**, 3723–3726.
[21] C. B. Anderson, A. B. S. Elliott, J. E. M. Lewis, C. J. McAdam, K. C. Gordon, J. D. Crowley, *Dalton Trans.* **2012**, *41*, 14625–14632.
[22] C. Achim, *J. Am. Chem. Soc.* **2005**, *127*, 1061–1061.
[23] in *Bond valence parameters*, *Vol.* **2011** https://www.iucr.org/resources/data/datasets/bond-valence-parameters.
[24] R. Bonetto, F. Crisanti, A. Sartorel, *ACS Omega* **2020**, *5*, 21309–21319.
[25] a) M. Abdinejad, A. Seifitokaldani, C. Dao, E. H. Sargent, X.-a. Zhang, H. B. Kraatz, *ACS Appl. Energ. Mater.* **2019**, *2*, 1330–1335; b) B. M. Ceballos, J. Y. Yang, *Proc. Natl. Acad. Sci. USA* **2018**, *115*, 12686–12691; c) K. M. Waldie, A. L. Osterichter, M. H. Reineke, A. F. Sasayama, C. P. Kubiak, *ACS Catal.* **2018**, *8*, 1313–1324; d) S. Dey, T. K. Todorova, M. Fontecave, V. Mougel, *Angew. Chem. Int. Ed.* **2020**, *59*, 15726–15733; *Angew. Chem.* **2020**, *132*, 15856–15863.
[26] Z.-C. Fu, C. Mi, Y. Sun, Z. Yang, Q.-Q. Xu, W.-F. Fu, *Molecules* **2019**, *24*.
[27] a) E. Alberico, S. Möller, M. Horstmann, H.-J. Drexler, D. Heller, *Catalysts* **2019**, *9*, 582; b) S. Gonell, J. Lloret-Fillol, A. J. M. Miller, *ACS Catal.* **2021**, *11*, 615–626.
[28] a) Y. Pellegrin, F. Odobel, *C. R. Chim.* **2017**, *20*, 283–295; b) Y. Tamaki, K. Koike, O. Ishitani, *Chem. Sci.* **2015**, *6*, 7213–7221.
[29] A. Barbieri, G. Accorsi, N. Armaroli, *Chem. Commun.* **2008**, *19*, 2185–2193.
[30] C. G. Kalodimos, I. P. Gerothanassis, A. Troganis, B. Loock, M. Momenteau, *J. Biomol. NMR* **1998**, *11*, 423–435.
[31] Y. Tamaki, K. Koike, T. Morimoto, O. Ishitani, *J. Catal.* **2013**, *304*, 22–28.
[32] J. L. Burmeister, F. Basolo, *Inorg. Chem.* **1964**, *3*, 1587–1593.
[33] a) A. M. Masdeu-Bultó, M. Reguero, C. Claver, *Eur. J. Inorg. Chem.* **2022**, e202100975; b) G. Dai, J. Liu, *J. Mater. Sci.* **2020**, *55*, 14301–14314.
[34] a) A. Becke, *Chem. Phys.* **1990**, *90*, 5648; b) A. Schäfer, H. Horn, R. Ahlrichs, *J. Chem. Phys.* **1992**, *97*, 2571–2577; c) A. Schäfer, C. Huber, R. Ahlrichs, *J. Chem. Phys.* **1994**, *100*, 5829–5835.
[35] a) S. Straub, P. Brunker, J. Lindner, P. Vohringer, *Angew. Chem. Int. Ed.* **2018**, *57*, 5000–5005; *Angew. Chem.* **2018**, *130*, 5094–5099; b) S. Straub, P. Vohringer, *Angew. Chem. Int. Ed.* **2021**, *60*, 2519–2525; *Angew. Chem.* **2021**, *133*, 2549–2555.
[36] A. Chapovetsky, M. Welborn, J. M. Luna, R. Haiges, T. F. Miller III, S. C. Marinescu, *ACS Cent. Sci.* **2018**, *4*, 397–404.
[37] G. Frenking, I. Fernández, N. Holzmann, S. Pan, I. Krossing, M. Zhou, *JACS Au* **2021**, *1*, 623–645.
[38] M. Loipersberger, D. G. Cabral, D. B. Chu, M. Head-Gordon, *J. Am. Chem. Soc.* **2021**, *143*, 744–763.
[39] a) R. N. Sampaio, D. C. Grills, D. E. Polyansky, D. J. Szalda, E. Fujita, *J. Am. Chem. Soc.* **2020**, *142*, 2413–2428; b) H. Koizumi, H. Chiba, A. Sugihara, M. Iwamura, K. Nozaki, O. Ishitani, *Chem. Sci.* **2019**, *10*, 3080–3088.
[40] TURBOMOLE V7.5 2020, a development of University of Karlsruhe and Forschungszentrum Karlsruhe GmbH, 1989–2007, TURBOMOLE GmbH, since **2007**; available from https://www.turbomole.org.
[41] S. G. Balasubramani, G. P. Chen, S. Coriani, M. Diedenhofen, M. S. Frank, Y. J. Franzke, F. Furche, R. Grotjahn, M. E. Harding, C. Hattig, A. Hellweg, B. Helmich-Paris, C. Holzer, U. Huniar, M. Kaupp, A. Marefat Khah, S. Karbalaei Khani, T. Muller, F. Mack, B. D. Nguyen, S. M. Parker, E. Perlt, D. Rappoport, K. Reiter, S. Roy, M. Ruckert, G. Schmitz, M. Sierka, E. Tapavicza, D. P. Tew, C. van Wullen, V. K. Voora, F. Weigend, A. Wodynski, J. M. Yu, *J. Chem. Phys.* **2020**, *152*, 184107.
[42] S. Grimme, A. Hansen, S. Ehlert, J. M. Mewes, *J. Chem. Phys.* **2021**, *154*.
[43] E. Caldeweyher, S. Ehlert, A. Hansen, H. Neugebauer, S. Spicher, C. Bannwarth, S. Grimme, *J. Chem. Phys.* **2019**, *150*, 154122.
[44] H. Kruse, S. Grimme, *J. Chem. Phys.* **2012**, *136*, 04B613.
[45] F. Weigend, R. Ahlrichs, *Phys. Chem. Chem. Phys.* **2005**, 7, 3297–3305.
[46] a) N. Frank, *WIREs Comput. Mol. Sci.* **2012**, *2*, 73–78; b) F. Neese, *Comput. Mol. Sci.* **2018**, *8*(1), 6.

Manuscript received: September 26, 2022
Revised manuscript received: October 6, 2022
Accepted manuscript online: October 7, 2022
Version of record online: ■■, ■■■

RESEARCH ARTICLE

Carbon dioxide reduction: A new heteroleptic iron complex can produce carbon monoxide from CO_2 via photo-driven catalysis, induced by a Cu^{I}-photosensitizer. This earth-abundant system gives CO with a turnover number of 576 and a quantum yield up to 7%. Competitive H_2 formation leads to syngas generation. This accomplishment is a further step toward sustainable CO_2 employment.

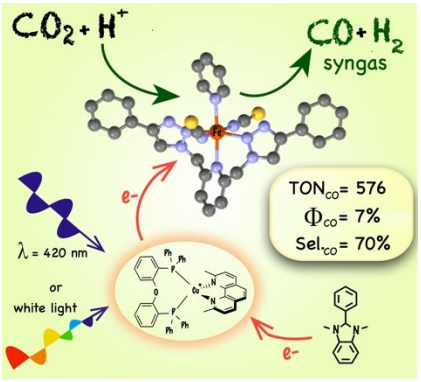

*L.-L. Gracia, E. Barani, J. Braun, A. B. Carter, Dr. O. Fuhr, Prof. A. K. Powell, Prof. Dr. K. Fink, Dr. C. Bizzarri**

1 – 12

Photocatalytic Reduction of CO_2 by Highly Efficient Homogeneous Fe^{II} Catalyst based on 2,6-Bis(1′,2′,3′-triazolyl-methyl)pyridine. Comparison with Analogues.